Niobium Pentoxide Thin Film Prepared using Simple Colloidal Suspension for Optoelectronic Application

M. K. Abood[1,2], E. T. Salim[1*] and J. A. Saimon[1]

[1]*Department of Applied Science, University of Technology, 10001 Baghdad, Iraq.*
[2] *Energy and Renewable Energies Technologies Center.*

ABSTRACT

In this study, thin-film microstructures of polymorphous niobium pentoxide were successfully prepared at a low temperature. Spin coating was employed to deposit the colloidal suspension before and after ultrasonic vibration. The deposited films were characterised and analysed by X-ray diffraction, scanning electron microscopy, and spectrophotometry for optical investigation. Results show that the films prepared before ultrasonic vibration possess a smooth and uniform surface. By contrast, films that underwent further ultrasonic vibration exhibit an earth rock-like structure and a highly oriented, void- and crack-free surface. Both film structures indicate the formation of a monoclinic structure. Low energy gap values of approximately 2.5 eV and 2.25 eV are suitable for heterojunction optoelectronic applications; this condition was proven by the typical I-V behaviours of the prepared heterojunction on the silicon substrate.

Keywords: Nb_2O_5, Thin Films, Scanning Electron Microscopy (SEM), Sol–Gel Method, Niobic Acid, Colloidal Solution.

1. INTRODUCTION

As a Group Five transition element, niobium fundamentally subsists in a minimum of four stable stoichiometric oxide forms, namely NbO, Nb_2O_3, NbO_2 and Nb_2O_5. Each of these oxide forms possesses several electrical properties ranging from conduction to semiconduction and insulation [1, 2].

Thermodynamically, niobium pentoxide (Nb_2O_5) is a highly stable form [3]. This material possesses semiconducting property and is known as an *n*-type semiconductor with a band gap of approximately 3.4 eV, depending on the structure and the preparation method [4-6]. Nb_2O_5 has gained considerable research attention because of its numerous distinct physicochemical properties and structural isotropy [7-14]; these properties make Nb_2O_5 appropriate for numerous applications, such as catalysts, solar cells, gas sensors, optical filters, electrochromic and magnetic devices, biotechnology and nanotechnology, and photoelectrodes and optoelectronics [15-17].

Nb_2O_5 subsists in numerous polymorphic shapes depending on the temperature at which the material is crystallised. The amorphous phase starts to crystallise in the TT-Nb_2O_5 (pseudo-hexagonal) form at a low temperature of approximately 500°C; the T-Nb_2O_5 (orthorhombic) structure is achieved at a high preparation temperature ranging from 600°C to 800°C; H-Nb_2O_5 (monoclinic structure) phase originates from heating to approximately 1100°C in air. The
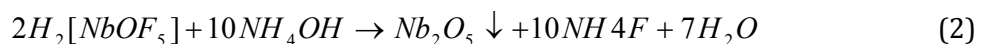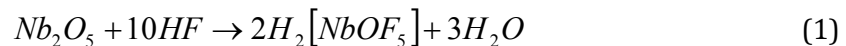
---

crystalline attitude of this material is affected by the raw materials used, synthesis processes, potential impurities and any interaction with other components [18-20]. Oxygen content is another critical property that influences the prepared Nb_2O_5 film structure. At low oxygen content, the film structure is in the TT crystalline phase, whereas $H-Nb_2O_5$ presents the highest oxygen content [21]. The development of niobium oxide thin films [22] or nanoparticles [6, 23] show extensive potential applications, so different preparation methods such as pulse laser deposition, electrodeposition, and sol–gel method have been employed [24, 25]. The sol–gel method offers numerous advantages compared to other methods, such as the flexibility to produce thin or thick films depending on the deposition condition. Examples of sol–gel application include thin films used as bond coating to increase adhesion between layers and thick films used as a corrosion protection layer, which produce a complex shape geometry in gel state. Thus, the sol–gel method is a simple, economical, and efficient method to produce high-purity films [26].

Ultrasonic vibration can be employed to improve the structural, morphological, and optical properties of the prepared thin film. This improvement can be achieved by increasing the homogeneity, stoichiometry, and crystallinity of the colloidal solution. This method can also be used for cleaning because it can rapidly reach a high temperature and pressure during ultrasonication, and ultrasound causes a resonant impinging effect on the solids [27, 28]. In this work, a niobic acid-based colloidal solution was obtained by sol–gel method and successfully deposited by spin coating.

This study focuses on a low-temperature preparation of $H-Nb_2O_5$ thin films without post heat treatment in addition to the use of a new raw material, which has not been applied in Nb_2O_5 thin-film preparation to the best of our knowledge.

2. EXPERIMENT

The required Nb_2O_5 colloidal solution was obtained using $M-Nb_2O_5$ powder (ultra purity, 99.99%), hydrofluoric acid, and ammonia without further purification. The reagents were mixed at a 1:1:4:8 molar ratio of DIW, ethanol, HF and NH_3OH, with 0.2g Nb_2O_5 powder. Hydrofluoric acid and Nb_2O_5 were mixed while being heated and stirred for 1 hour until a transparent solution was obtained. Afterward, ammonia, water, and ethanol were added while being continuously stirred for 1 hour in a 100°C water bath. A milky colloidal solution was obtained. An ultrasonic vibration instrument (Microelectronic brain control 3560) was used with an operating power of 50 W for 30 min. Chemical reactions in previous studies usually take the following chemical formula [29, 30]:

$$Nb_2O_5 + 10HF \rightarrow 2H_2[NbOF_5] + 3H_2O \tag{1}$$

$$2H_2[NbOF_5] + 10NH_4OH \rightarrow Nb_2O_5 \downarrow + 10NH4F + 7H_2O \tag{2}$$

Spin coating was employed to obtain homogeneous Nb_2O_5 thin films. The colloidal solution was deposited on quartz substrates at a rotational speed of 2500 rpm for 1 min. The films were prepared before and after ultrasonic vibration. After deposition, films were dried at 100°C for 5 min in static air. No further heat treatment was conducted. A T60 UV–vis spectrophotometer was used to measure the optical properties of the prepared films. The energy gap was determined using the following equation:

$$(\alpha h\nu) = A(h\mu - Eg)^{1/2} \tag{3}$$

where α is the absorption coefficient, $h\nu$ is the energy of the incident photon, A is a constant, and E_g is the optical band gap. The value of α can be obtained depending on the film thickness t and its transmittance T by using the following equation:

$$\alpha = \frac{1}{t}\ln\frac{1}{T} \tag{4}$$

The band gap of the prepared thin films was obtained by extending the straight line of the $(\alpha h\nu)^2$–$h\nu$ plot with the incident photon energy. Structural properties were obtained using Cu-kα X-ray source from Shimadzu 6000. Grain size D, density of dislocation δ, and strain ε were measured based on the X-ray diffraction (XRD) result by using the following equations:

$$D = \frac{K\lambda}{\beta\cos\theta} \tag{5}$$

$$\delta = \frac{1}{D^2} \tag{6}$$

$$\varepsilon = \frac{\beta}{4\tan\theta} \tag{7}$$

where λ is the used wavelength, β is the full width at half maximum and θ is Bragg's angle [31]. A scanning optical reflectometer (Filmetrics F20, USA) was used for film thickness measurement. Then, morphological properties were obtained using an AA-3000-type scanning electron microscope.

3. RESULTS AND DISCUSSION

Figure 1 shows the absorption spectra of the Nb_2O_5 thin films prepared on quartz substrates before and after ultrasonic vibration. The plotted absorption spectrum within a spectral range of 300–1000nm increases after ultrasonic vibration owing to the increase in film thickness, which may be attributed to the increase in the number of Nb_2O_5 microparticles. Thus, the density in the unit volume of the colloidal suspension (which was subsequently deposited on a quartz substrate) increases. These results are consistent with those of previous studies [32, 33].

The film thickness was measured to be approximately 430 and 460nm for samples deposited before and after ultrasonic vibration, respectively; this result indicates the increase in the absorbance results of the prepared films. Optical results show a sharp band edge absorption in the UV region for all prepared films, which indicates that the obtained energy gap values rely on a direct band gap semiconductor mathematical model, as expressed in equation 3 and shown in Figure 2.

Figure 2 shows the obtained E_g values. The values are low compared with the band gap values of the corresponding Nb_2O_5 films obtained using other chemical methods. The values were approximately 2.5 and 2.25 eV for samples prepared before and after ultrasonic vibration, respectively. This result may be attributed to the presence of a sup band in the electronic structure associated with the prepared microstructure films. This result coincides with the scanning electron microscopy (SEM) results, which indicate the formation of a microstructure thin film; a previous study also obtained similar results [34]. The energy gap value generally increases with molar concentration; in this case, the decrease in energy gap values corresponds

to the increase in particle grain size after ultrasonic vibration, which is in agreement with the SEM results.
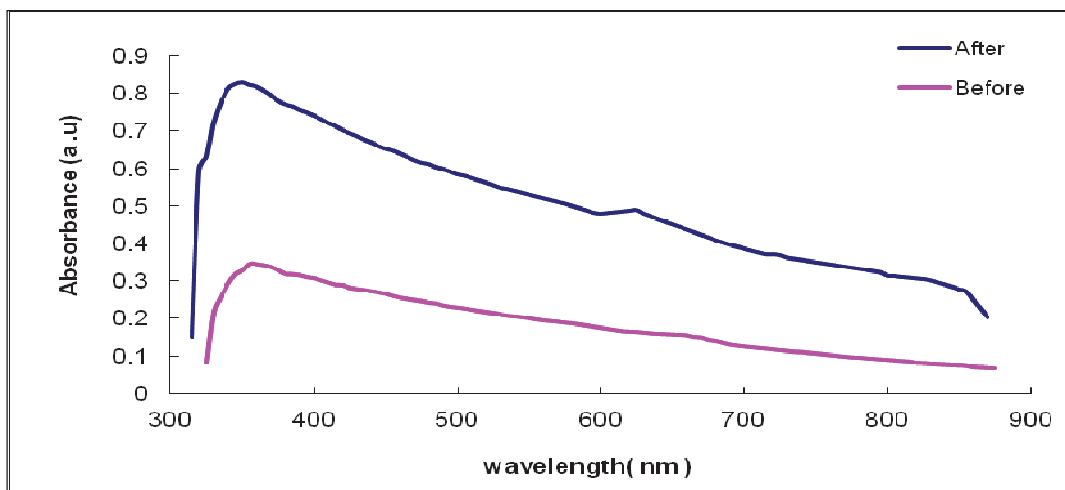

Figure 1. Absorption as a function of wavelength for Nb_2O_5 thin films prepared before and after ultrasonic vibration.
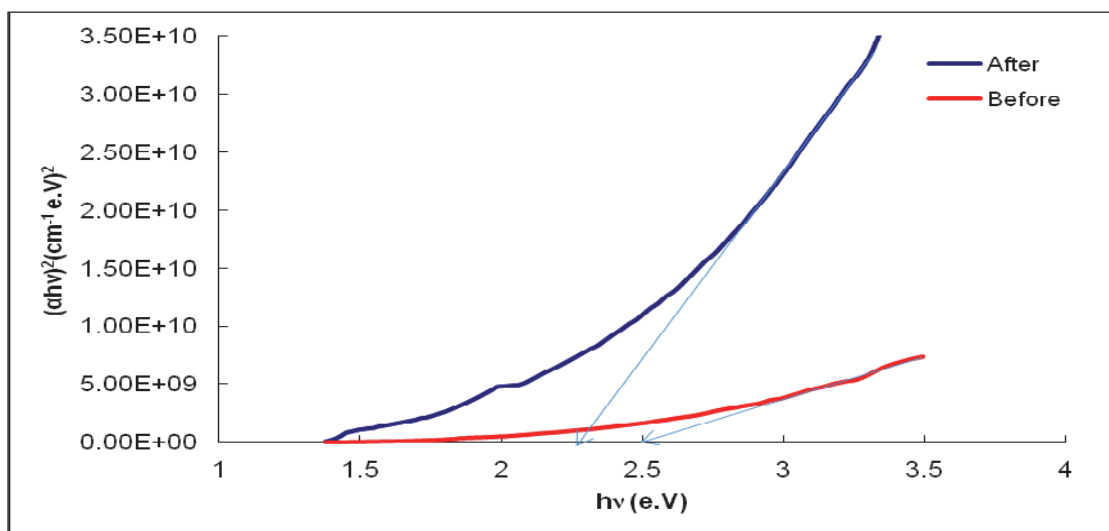

Figure 2. Estimated energy gap values for prepared Nb_2O_5 thin films before and after ultrasonic vibration.

The XRD results of the prepared films on quartz substrate before and after ultrasonic vibration are presented in Figure 3.

All peaks of Nb_2O_5 films correspond to the peaks of JCPDF card file 00-037-1468. The diffraction peaks in both cases suggest the successful formation of H-Nb_2O_5 thin films with a clear polymorphous structure. The synthesis of this structure may be attributed to the abundant oxygen in the suspension coming from the decomposition of H_2O and ethanol during chemical reaction; the abundant oxygen thus increases the oxygen content in the prepared structure, producing H-Nb_2O_5; a previous study obtained similar results [21]. This condition may also be correlated with the transformation of the raw material structure from the M-Nb_2O_5 structure of the used powder, which is assumed to be a disordered or poorly crystalline H in H-Nb_2O_5 after an appropriate heat treatment in water bath during production; this result was confirmed by a previous study [35].

The diffraction peaks at 2θ = (14.2, 17, 18.4, 20.4, 37.2 and 43.2) are ascribed to the Nb_2O_5 diffraction plane values of 203, 301, 403, −304, −610 and 017, respectively. The moderate diffraction peak for both samples prepared before and after ultrasonic vibration is at the 301 diffraction plane, suggesting the formation of a monoclinic crystalline structure. Figure 3 shows significant improvement in the structure of the prepared films after ultrasonic vibration, where the Nb_2O_5 diffraction peak appears at the 301 diffraction plane with doubled intensity compared with other diffraction peaks corresponding to the same material. This condition is associated with a relative reduction in NbO diffraction peaks compared with the related XRD peak belonging to the Nb_2O_5 diffraction plane for the same sample after ultrasonic vibration.
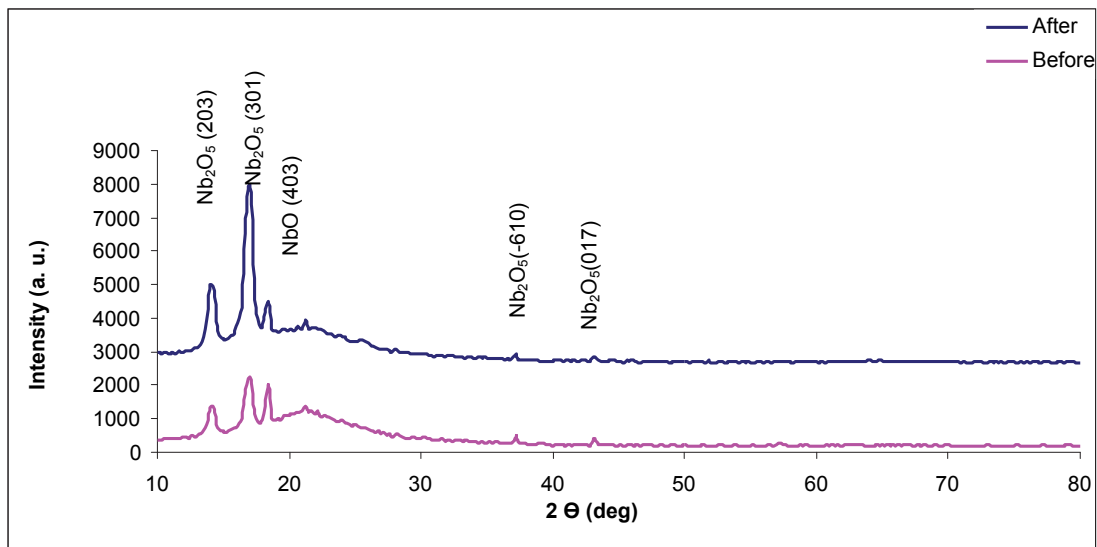

Figure 3. X-ray diffraction results of prepared thin films after and before ultrasonic vibration process.

As shown in Table 1, D, ε, β and δ improve the crystallisation property and the reduced film defects by increasing the grain size and reducing the dislocation density and strain values after ultrasonic vibration [36].

Table 1 Structural parameters of prepared films

Peaks	Before ultrasonic vibration process				After ultrasonic vibration process			
	B (deg)	D (nm)	$(\delta)*10^{3-}$ (line/m^2)	ε	B (deg)	D (nm)	$(\delta)*10^{-3}$ (line/m^2)	E
14.2	1.0	8.4	14.29	10.04	0.6	13.9	5.1	6.0
17.0	1.0	8.7	13.07	0.74	0.7	12.0	7.0	0.5
18.4	0.1	18.0	3.09	0.24	0.4	21.0	2.3	0.7
Average	0.7	11.7	10.15	3.67	0.6	15.7	4.8	2.4

The morphological properties of both Nb_2O_5 thin films prepared before and after ultrasonic vibration are shown in the SEM micrograph in Figures 4a and 4b respectively. The micrographs clearly show that film homogeneity decreases after ultrasonic vibration, owing to the increase in the amount of Nb_2O_5 microparticles in the colloidal suspension, which tend to aggregate and form a material with a large grain size. Microstructures with an earth rock-like structure formed along the film surface. Such structure is a normal characteristic of films derived from sol–gel method [37]. The average grain sizes obtained from the SEM micrographs increased after ultrasonic vibration, owing to the increase in aggregation associated with Nb_2O_5 material concentration per unit volume of the colloidal suspension, and consequently, with film density

per unit area. The grains became denser after ultrasonic vibration, resulting in an increase in the thickness of the prepared films.
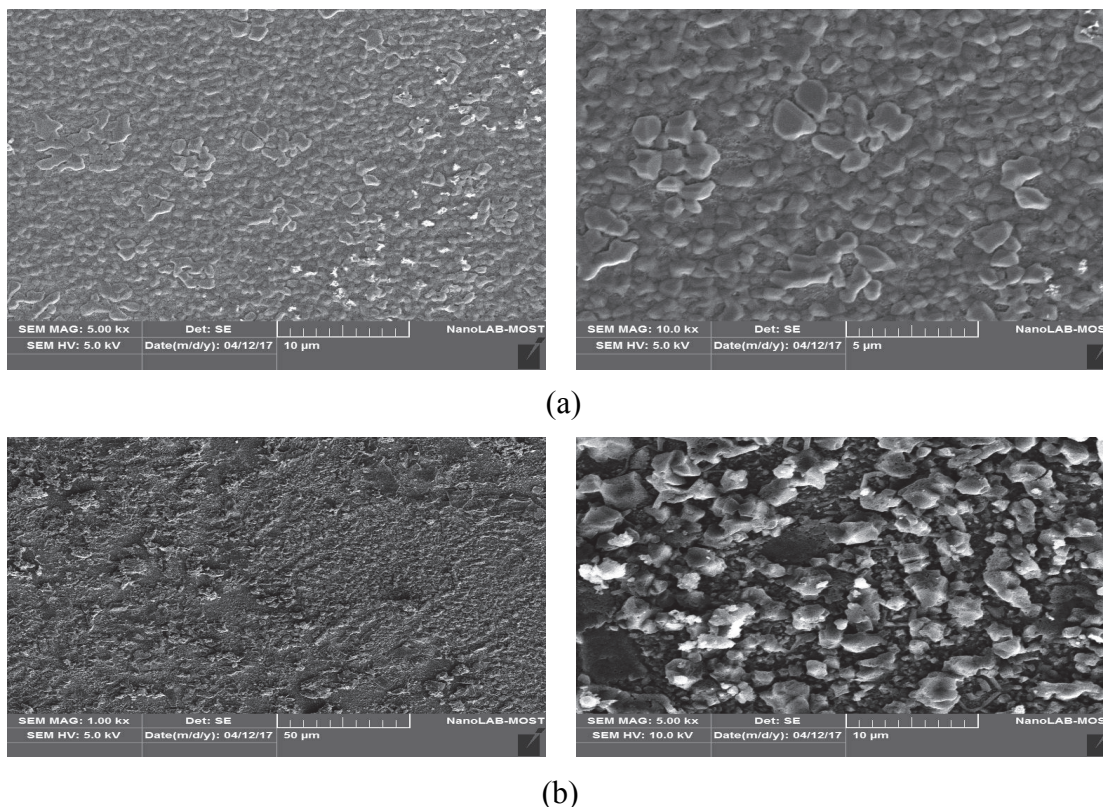

(a)

(b)

Figure 4. Scanning electron microscope micrograph represents prepared films before (a) and after (b) ultrasonic vibrational process.

To characterise the device as heterojunction, we prepared Nb_2O_5 films on the silicon substrate before and after ultrasonic vibration.

Figure 5 reveals a clear enhancement in the forward and reverse current characteristics after ultrasonic vibration. The current–voltage characteristic in the forward current is shown in two significant regions, namely recombination and tunnelling current regions. The forward current after ultrasonic vibration significantly increased in the two regions; this increase may be attributed to the increase in the number of electron–hole pairs generated due to the increase in colloidal density, that is, the number of molecules per unit volume. Consequently, the increase results in the increase of the number of electron–hole pairs generated and drifting in the specifically applied bias. The significant increase in the forward current is also due to the increase in film thickness after ultrasonic vibration, which is related to the reduced thickness of the depleted region. The apparent barrier height is attributed to the increase in saturated current density. A previous study confirmed this result [38]. Similar to the forward current, the reverse current increased substantially after ultrasonic vibration; the curve also presents two regions. The generated current slightly increased with the applied voltage as a result of the generation of electron–hole pairs at low voltage bias. The increase in the second region is correlated with the diffusion of minority carriers through the junction.

Device rectification also increased due to the increase in the interstitial site, which resulted in large generation–recombination and diffusion currents.
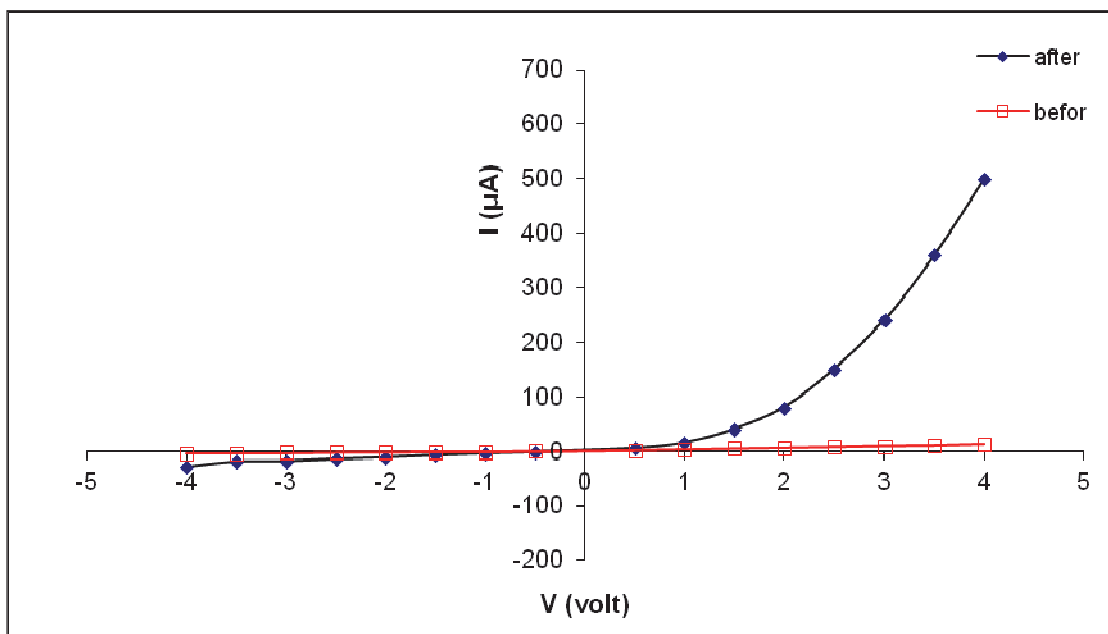
Figure 5. Current–voltage characteristics of Nb_2O_5 thin films deposited into silicon substrates before and after ultrasonic vibration.

4. CONCLUSIONS

Nb_2O_5 thin films with relatively low band gap values were prepared successfully by using niobic acid-based colloidal solution as a raw material. Homogenous crack-free thin films were obtained via spin coating before and after ultrasonic vibration. The structural properties reveal the successful formation of the monoclinic structure at low temperature and in the absence of post heat treatment. The obtained optical band gap values decreased from 2.5 eV to 2.25 eV after ultrasonic vibration. The electrical properties of the forward and reverse bias demonstrate the potential of the prepared device for photovoltaic applications.

REFERENCES

[1]   M. A. Aegerter, Solar Energy Materials and Solar Cells **68** (2001) 401.
[2]   K. Tanabe, Catalysis Today **78** (2003) 65.
[3]   Sv. Ganev , S. Parvanov , S. Slavov , A. Bachvarova-Nedelcheva, R. Iordanova, Y. Dimitriev, Bulgarian Chemical Communications **49** (2017) 103.
[4]   J. Gandhi, R. Dangi, S. Bhardwaj, Rasayan J. Chem **1** (2008) 567.
[5]   H. Y. Lin, H. C. Yang, W. L. Wang, Catalysis Today **174** (2011) 106.
[6]   M. R. Joya, J. J. B Ortega, A. M. Raba, J. G. S. Filho, P. T. Freire, Metals, 142 **(**2017) 2.
[7]   Y. S. Huang, Y. Z. Zhang, X. F. Hu, Journal of Inorganic Materials **17** (2002) 632.
[8]   S. Sathasivam , B. A. D. Williamson, S. A. Althabaiti, A. Y. Obaid, S. N. Basahel, M. Mokhtar, D. O. Scanlon, C. J. Carmalt , I. P. Parkin, ACS Appl. Mater. Interfaces **9** (2017) 18031.
[9]   S. H. Mujawar, A. I. Inamdar, C. A. Betty, V. Ganesan, P. S. Patil, Electro chemical Acta **52** (2007) 4899.
[10] L. G. Luciana, V. S. G. F. D. HotzaJairo, A. E. João, B. R, N. Carlos, R. Rambo, Journal of Sol-Gel Science and Technology **83** (2017) 537.
[11] A. G. S. Prado, L. B. Bolzon, C. P. Pedroso, A. O. Moura, L. L. Costa, Applied Catalysis B Environmental **82** (2008) 219.

[12] P. Carniti, A. Gervasini, M. Marzo, The Journal of Physical Chemistry C. **112** (2008) 14064.

[13] T. Sreethawong, S. Ngamsinlapasathian, S. H. Lim and S. Yoshikawa, Chemical Engineering Journal **215** (2013) 322.

[14] M. L. Marin, G. L. Hallett-Tapley, S. Impellizzeri, C. Fasciani, S. Simoncelli, J. C. Netto-Ferreira, Catalysis Science & Technology **4** (2014) 3044.

[15] G. Falk, M. Borlaf, M. J. López-Muñoz, J. C. Fariñas, J. B. R. Neto, R. Moreno, Get access **32** (2017) 3271.

[16] M. R. Angela, B. R. Jorge, R. J. Miryam, Mat. Res. **19** (2016) 1381.

[17] K. Lazarova, M. Vasileva, G. Marinov, T. Babeva, Optics & Laser Technology **58** (2014) 114.

[18] G. Ramírez, S. E. Rodil, S. Muhl, D. Turcio-Ortega, J. J. Olaya, M. Rivera, E. Camps, L. Escobar-Alarcón, Journal of Non-Crystalline Solids **356** (2010) 2714.

[19] A. L. Viet, M. V. Reddy, R. Jose, B. V. R. Chowdari, S. Ramakrishna, J. Phys. Chem. C **114** (2010) 664.

[20 J. K. Dash, L. Chen, Michael R. Topka, Peter H. Dinolfo, L. H. Zhang, K. Kiss linger, T.-M. Lua, G.-C. Wang, RSC Adv. **5** (2015) 36129.

[21] M. A. Aegerter" Solar Energy Materials & Solar Cells **68** (2001) 401 422.

[22] A. M. Raba, J. Bautista, E. Murillo, Journal of Physics: Conference Series **687** (2016) 012084.

[23] Y. Zhou, Z. Qiu, M. Lu, A. Zhang, Q. Ma, Journal of Luminescence **128** (2008) 1369.

[24] E.T. Salim, M. A. Fakhri, H. Hassen, Int. J. Nanoelectronics and Materials **6** (2013) 121.

[25] U. Pirnat, M. Valant, B. Jančar, D. Suvorov, Chem. Mater. **17** (2005) 5155.

[26] Qi Tang, H. Zhu, C. Chen , Y. Wang , Z. Zhu, J. Wu, W. Shih, Materials Research **20** (5) (2017) 1340.

[27] A. I. Oliva, R. Castro-Rodríguez, O. Solís-Canto, V. Sosa, P Quintana, J. L. Peña, Applied surface science **205** (2003) 56.

[28] Evan T. Salim, Raid A. Ismail, Makram A. Fakhry. Yushamdan Yusof, Int. J. Nanoelectronics and Materials **9** (2016) 111.

[29] Makram A Fakhri, Int. J. Nanoelectronics and Materials **9** (2016) 93.

[30] N. Izabela, Z. Maria, Chemical Reviews **99** (1999) 3603.

[31] A. Singh, H.L. Vishwakarma, Materials Science-Poland **33** (2015) 751.

[32] E. T. Salim, Int.J. Nanoelectronics and materials (IJNeaM) **5** (2012) 95.

[33] Zaid T Salim, U Hashim, MK Md Arshad, Makram A Fakhri, Evan T Salim, Materials Research Bulletin **86** (2017) 215.

[34] E. T. Salim, J. A. Saimon, M. K. Abood, M. A Fakhri, Mater. Res. Express **4** (2017) 106407.

[35] E. I. KO, J. G . Weissman, Catalysis Today **8** (1990) 27-36

[36] F. M.˙Tezel, I. A. Kariper , Materials Science-Poland **35** (2017) 87.

[37] Makram A Fakhri, Y Al-Douri, Uda Hashim, Evan T Salim, Advanced Materials Research, **1133** (2016)457.

[38] E. T. Salim, M. S. AL Wazny M. A. Fakhri, Mod. Phys . Lett. B **27** (2013) 1350122.